

THz-Wave Generation in a Magnetoresistive Manganite

$\text{Pr}_{0.7}\text{Ca}_{0.3}\text{MnO}_3$

N. Kida and M. Tonouchi

Research Center for Superconductor Photonics, Osaka University

and Core Research for Evolutional Science & Technology (CREST), Japan Science & Technology Corporation (JST)

2-1 Yamadaoka, Suita, Osaka 565-0871, Japan

(December 2, 2024)

Abstract

We discovered the THz-wave generation from the voltage applied optical switching device made on a magnetoresistive manganite $\text{Pr}_{0.7}\text{Ca}_{0.3}\text{MnO}_3$ excited by the femtosecond optical pulses. Its spectrum extends up to 1 THz centered at around 0.2 THz. The generation efficiency (η) linearly depends on both external stimulation. It is also shown that η strongly depends on temperature and the trend of $\eta(T)$ reverses sign across the charge-orbital and spin ordering temperatures, respectively. The first observation of the THz-wave generation in this material having a perovskite structure opens a vast range of related materials for future optical devices.

75.30.Vn, 42.65.Re, 07.57.Hm

In recent years, a wide variety of generation methods to produce the THz-wave were developed using the photoconductive antenna fabricated on semiconductors [1,2]. Low-temperature grown GaAs (LT-GaAs) is widely used as the optical switching device owing to its fast carrier lifetime, good mobility, and high breakdown electric field [3]. The mechanism of the THz-wave generation in these materials can be understood in the following classical Maxwell's equation [3–6],

$$\mathbf{E} = -\frac{A}{4\pi\epsilon c^2 r} \sin \theta \frac{\partial \mathbf{J}}{\partial t} \propto \frac{\partial \sigma}{\partial t} \mathbf{V}, \quad (1)$$

where A is the excited area, ϵ the dielectric constant of material, c the light velocity, r the distance of the radiation field \mathbf{E} , θ the angle of the bow-tie, \mathbf{J} the current, σ the conductivity, and \mathbf{V} the applied voltage. Eq. (1) indicates that the transient current (a typical order of femtosecond) created by the ultra-fast optical pulses are accelerated by an electric field, which then generates the THz-wave and is propagated into the free space.

Another materials had potential useful characters as described above is a strong correlated electron system like transition metal oxides with a perovskite structure. On the contrary, in the case of semiconductors the underlying physics in these materials is quite different as a result of the strong electron-electron Coulomb repulsion, which leads to the breaking of the single-particle approximation. Especially, hole-doped manganites with general formula $A_{1-x}B_x\text{MnO}_3$ (where A and B being rare-earth and alkaline-earth elements, respectively), have a rich variety of electronic and magnetic properties including colossal magnetoresistance phenomena [7–10].

Among them, $\text{Pr}_{1-x}\text{Ca}_x\text{MnO}_3$ system show distinct and unique features as compared to the canonical double-exchange ferromagnetic system $\text{La}_{1-x}\text{Sr}_x\text{MnO}_3$ [11]. $\text{Pr}_{1-x}\text{Ca}_x\text{MnO}_3$ with $x = 0.3 \sim 0.5$ exhibits insulating behavior; 1:1 charge and orbital ordering occur at $T_{\text{CO/OO}}$ and CE-type antiferromagnetic ordering develops below T_{N} [12,13]. In $\text{Pr}_{0.7}\text{Ca}_{0.3}\text{MnO}_3$, excess electrons are doped in Mn^{4+} , the ground-state transforms to the charge-orbital ordered spin-canted antiferromagnetic insulator below T_{CA} [12]. This charge-orbital ordered antiferromagnetic insulating phase of $\text{Pr}_{0.7}\text{Ca}_{0.3}\text{MnO}_3$ can be easily melted to

the charge-orbital disordered ferromagnetic metallic one by external perturbations such as magnetic field [11], stress field [14], electric field [15], X-ray illumination [16,17], and visible-light illumination under an electric field [18–21] and a magnetic field [22]. This transition is accompanied by more than 10 orders of magnitude change of the electrical resistance. Due to the metamagnetic transition, $\text{Pr}_{0.7}\text{Ca}_{0.3}\text{MnO}_3$ favors the acceptance of external perturbations. Besides, recent spectroscopic studies using pump-probe technique revealed that the fast optical response begins at a characteristic time of 230 femtosecond [23]. These complex features provide us another functionality of manganites; according to eq. (1), it is expected that the THz-wave can also be generated from $\text{Pr}_{0.7}\text{Ca}_{0.3}\text{MnO}_3$, but its mechanism is basically different from semiconductors, i.e., the ultra-fast optical modulation of the charge, spin and orbital ordering may be responsible for this effect. In this Letter, we show the first finding of the THz-wave generation from $\text{Pr}_{0.7}\text{Ca}_{0.3}\text{MnO}_3$. We also describe how the characteristics of the THz-wave vary with external stimulation.

We prepared a thin film of $\text{Pr}_{0.7}\text{Ca}_{0.3}\text{MnO}_3$ grown on $\text{MgO}(100)$ substrate by pulsed laser deposition technique. An X-ray diffraction analysis indicates that a film is *a*-axis oriented perpendicular to the MgO surface and has a lattice constant of 3.86 Å. Using conventional photolithographic techniques, we formed the optical switching structure coupled to a bow-tie antenna fabricated on $\text{Pr}_{0.7}\text{Ca}_{0.3}\text{MnO}_3$. The bow-tie antenna consists of 3 mm long and 200 μm wide gold lines with a gap of 5 μm and a bow-angle of 60°.

THz-wave generation and detection system is as follows. A mode-locked Ti:Sapphire laser operating at repetition rate of 82 MHz was used to generate the 80 femtosecond optical pulses at the wavelength of 800 nm (1.55 eV), which exceeds the charge-gap energy ~ 0.5 eV and nearly corresponds to the charge transfer energy from O 2p to Mn 3d band [24]. The pump-pulse was mechanically chopped at 2 kHz. A femtosecond optical pulses were focused into 30 μm in diameter by an object lens on the gap of the bow-tie antenna. In order to enhance the collection efficiency of the THz-wave, we attached an MgO hemispherical lens on the backside of MgO substrate. Propagated THz-wave was collimated and focused by a pair of off-axis paraboloidal mirrors. The bow-tie antenna detector was made of Au/Ge/Ni

alloy lines fabricated on LT-GaAs film. It consists of two parallel 20 mm long and 25 μm wide lines separated by 1 mm with a gap of $5 \times 5 \mu\text{m}$. The bow-angle is 60° . To measure the waveform in the time-domain, a part of the main laser light was split by a beam splitter and focused onto the bow-tie antenna detector after a time-delay. It becomes instantaneously conductive when hit by the optical pulse and detects a photocurrent caused by the electric field of the THz-wave. The time resolution is ~ 300 femtosecond and is determined mainly by the carrier lifetime of LT-GaAs.

We then discovered the THz-wave generation from $\text{Pr}_{0.7}\text{Ca}_{0.3}\text{MnO}_3$; the generated electromagnetic waveforms under the applied voltage of ± 32 V and the pump-pulse energy of 184 mW taken at 23 K are plotted in Fig. 1(a). The main peaks were observed around 24 ps (time-delay is arbitrary units). The pulsedwidth (full-width at half maximum of the main peak) is estimated to be 1 ps using a Gaussian profile to fit the data. The oscillation structures after the main peak are mainly due to multiple reflections of MgO substrate. By changing the polarity of the applied voltage, the propagated waveform reverses. It is necessary for both the applied voltage and the illumination of the femtosecond optical pulses to generate the THz-wave. These observations remind us of eq. (1), namely \mathbf{E} is proportional to the first derivative of \mathbf{J} . In other words, the transient current modulated by the femtosecond optical pulses are accelerated by the applied electric field.

To see the frequency profile, the time-domain waveforms for the applied voltage of ± 15 V in Fig. 1(a) were Fourier transformed to the frequency-domain. The obtained amplitude spectrum is shown in Fig. 1(b). It extends to ~ 1 THz centered at around 0.2 THz. The dips due to the absorption around 0.1 and 0.18 THz are seen in the spectrum, but the origin of these structures is not clear at present. The oscillating structure arising from the effect of multiple reflections of MgO substrate is also seen.

To get the detailed characteristics of the THz-wave generation, we measured the propagated THz-wave as a function of the pump-pulse energy at the fixed applied voltage of ± 15 V. The main peak amplitude was found to be a linear function of the pump-pulse energy as shown in Fig. 2(a) by solid squares. Solid lines in Fig. 2 show the least-squares fit of

the data, assuming the linear response as a function of both external stimulation. We found that all the data depending on the polarity of the applied voltage, can be well described by the linear relation $\sim P/(1+P)$, where P is a normalized laser intensity at small pump-pulse energy region [3–6]. This relation is well known to be the current surge model as the origin of the THz generation from semiconductors. The result of the main peak amplitude dependence of the applied voltage at the fixed pump-pulse energy of 122 mW is also encouraging in this picture; it was confirmed that the main peak amplitude linearly depends on the applied voltage [Fig. 2(b)].

These phenomena are not due to the local heating effect by the strong field caused by both the femtosecond optical pulses and the applied voltage, because the main peak amplitude of the THz-wave as a function of temperature changes around the electronic and magnetic transition temperatures as will be shown later. We also ruled out the possibility of the occurrence of the persistent insulator-metal transition due to the following reasons [18–21]. First, we did not observe the threshold behavior which is a typical feature of the photo-induced transition as shown in Figs. 2(a) and (b) [25]. Second, more clearly, we did not detect the breakdown of the applied voltage during our measurements.

We point out that the area irradiated by the optical pulses transiently transforms to metallic paths. As shown in Fig. 1(a) for the case of the applied voltage of 32 V, the shape of the waveform around 34 ps reveres compared to the shape of the main peak; it has the down-convex shape, while the main peak has the up-convex one. A time-delay (t) of this peak after the main peak is 10 ps, which agrees with the round trip time of the multiple reflection of MgO substrate assuming the refractive index $n = 3.1$ and thickness $d = 0.5$ mm, via the relation $t = 2dn/c$. Based on this result, we assigned the peak around 34 ps to the reflection at the interface between $\text{Pr}_{0.7}\text{Ca}_{0.3}\text{MnO}_3$ and MgO substrate. Therefore, the change of the peak shape arises from the local metallic characteristic of $\text{Pr}_{0.7}\text{Ca}_{0.3}\text{MnO}_3$. Based on the above reasons, we conclude that in first approximation the THz-wave generation is caused by the acceleration of the photogenerated transient metallic paths according to eq. (1).

Despite the similarity of the THz-wave generation characteristics in semiconductors, the

classical picture based on eq. (1) seems incapable of explaining all our data as described below. Figure 3 shows the temperature dependence of the generation efficiency (η) defined as normalized the main peak amplitude at the applied voltage of 15 V and the pump-pulse energy of 100 mW at 23 K on heating runs. During heating process, the position of the sample moves due to the vibration of the cryostat. Therefore, we fixed a time-delay at the main peak in Fig. 1(a) and subsequently scanned the sample along the x and y direction at respective temperatures and the laser spot is tuned to the center of the gap between electrodes before experiments. As clearly seen, η shows strong and curious temperature dependence. The temperature variation of the absorption coefficient of this material is negligible at the center of the laser-wavelength used in the photoexcitation [24]. It tends to decrease as the temperature is increased around 120 K. At further increased temperatures, η monotonically increases up to 230 K. Even at room temperature, the THz-wave is clearly observed. These critical points are well related T_{CA} , T_{N} , and $T_{\text{Co/oo}}$ as previously reported values [11]. Moreover, the slope of $\eta(T)$ changes in reverse around these temperatures. The temperature dependence of η as followed that of σ is expected according to eq. (1), because the conventional picture of the THz-wave generation in semiconductors can be understand the first derivative of σ . Our sample used in this experiment shows the typical insulating behavior; it monotonically increases by four orders of magnitude from a low-temperature value to a room-temperature one and shows no clear correlation of the spin ordering as well as the charge-orbital ordering as shown in the inset of Fig. 3. This behavior cannot be explained using eq. (1) alone, which implies that the electronic as well as magnetic properties can strongly affect characteristics of the THz-wave generation, another mechanism on the basis of eq. (1) may be needed to understand this temperature behavior. To the best of our knowledge, THz-wave generation from magnetic materials has so far not been observed.

Our results described here open the door for investigations and future ultra-fast optical devices using magnetoresistive manganites. For future demands in these optical functionality combined with other exotic properties, other materials with a perovskite structure may show these characters in addition to their extraordinary properties such as ferroelectricity

and magnetism. Our spectrum described here in initial experiments is limited the frequency of the THz-wave up to 1 THz. Therefore, we will improve the antenna structure. Further experiments under a magnetic field are also interesting subjects. From viewpoints of studies of ultra-fast phenomena in manganites, characterizations of the THz-wave in the time-domain may be expected to give fruitful information in the underlying physics of manganites.

REFERENCES

- [1] A. Bonvalet and M. Joffre, in *Femtosecond Laser Pulses, Principles and Experiments*, edited by C. Rullière (Springer-Verlag, Heidelberg, 1998).
- [2] D. H. Auston, K. P. Cheung, and P. R. Smith, *Appl. Phys. Lett.* **45**, 284 (1984).
- [3] M. Tani, S. Matsuura, K. Sakai, and S. Nakashima, *Appl. Opt.* **36**, 7853 (1997).
- [4] A. J. Taylor, P. K. Benicewicz, and S. M. Young, *Opt. Lett.* **18**, 1340 (1993).
- [5] J. T. Darrow, X-C. Zhang, and D. H. Auston, *IEEE J. Quantum Electron.* **28**, 1607 (1992).
- [6] P. K. Benicewicz and A. J. Taylor, *Opt. Lett.* **18**, 1332 (1993).
- [7] *Colossal Magnetoresistive Oxides*, edited by Y. Tokura (Gordon and Breach Science, New York, 2000).
- [8] Y. Tokura, *JSAP International No. 2*, 12 (2000).
- [9] Y. Tokura and N. Nagaosa, *Science* **288**, 462 (2000).
- [10] Y. Tokura and Y. Tomioka, *J. Magn. Magn. Mater.* **200**, 1 (1999).
- [11] Y. Tomioka *et al.*, *Phys. Rev. B* **53**, R1689 (1996).
- [12] H. Yoshizawa, H. Kawano, Y. Tomioka, and Y. Tokura, *Phys. Rev. B* **52**, R13145 (1995).
- [13] M. v. Zimmermann *et al.*, *Phys. Rev. Lett.* **83**, 4872 (1999).
- [14] Y. Moritomo, H. Kuwahara, Y. Tomioka, and Y. Tokura, *Phys. Rev. B* **55**, 7549 (1997).
- [15] A. Asamitsu, Y. Tomioka, H. Kuwahara, and Y. Tokura, *Nature (London)* **388**, 50 (1997).
- [16] V. Kiryukhin *et al.*, *Nature (London)* **386**, 813 (1997).
- [17] D. Casa *et al.*, *Europhys. Lett.* **47**, 90 (1999).

- [18] K. Miyano, T. Tanaka, Y. Tomioka, and Y. Tokura, Phys. Rev. Lett. **78**, 4257 (1997).
- [19] M. Fiebig, K. Miyano, Y. Tomioka, and Y. Tokura, Science **280**, 1925 (1998).
- [20] M. Fiebig, K. Miyano, Y. Tomioka, and Y. Tokura, Appl. Phys. Lett. **74**, 2310 (1999).
- [21] K. Ogawa *et al.*, Phys. Rev. B **57**, R15033 (1998).
- [22] Y. Okimoto *et al.*, Mol. Cryst. Liq. Cryst. **315**, 257 (1998).
- [23] M. Fiebig, K. Miyano, Y. Tomioka, and Y. Tokura, J. Lumin. **87-89**, 82 (2000).
- [24] Y. Okimoto *et al.*, Phys. Rev. B **57**, R9377 (1998).
- [25] S. Koshihara, J. Lumin. **87-89**, 77 (2000).

FIGURES

FIG. 1. (a) The propagated THz-waveforms in the time-domain under the applied voltage of ± 32 V and the pump-pulse energy of 184 mW measured at 23 K. (b) Amplitude spectrum in the frequency-domain of the THz-wave in (a). Data is normalized with the value of the absolute maximum amplitude.

FIG. 2. Main peak amplitude as a function of (a) the pump-pulse energy at the fixed applied voltage of ± 15 V and (b) the applied voltage at the fixed pump-pulse energy of 122 mW measured at 23 K. Data is normalized with the value of the amplitude under the applied voltage of 15 V and the pump-pulse energy of 122 mW.

FIG. 3. Temperature dependence of the generation efficiency (η) at the fixed applied voltage of 15 V and the pump-pulse energy of 100 mW. $\eta = 1$ is defined the main peak amplitude at 23 K. Inset shows the logarithmic scale of the electrical resistance as a function of temperature measured at a constant current of 1 μ A with a four-probe configuration.

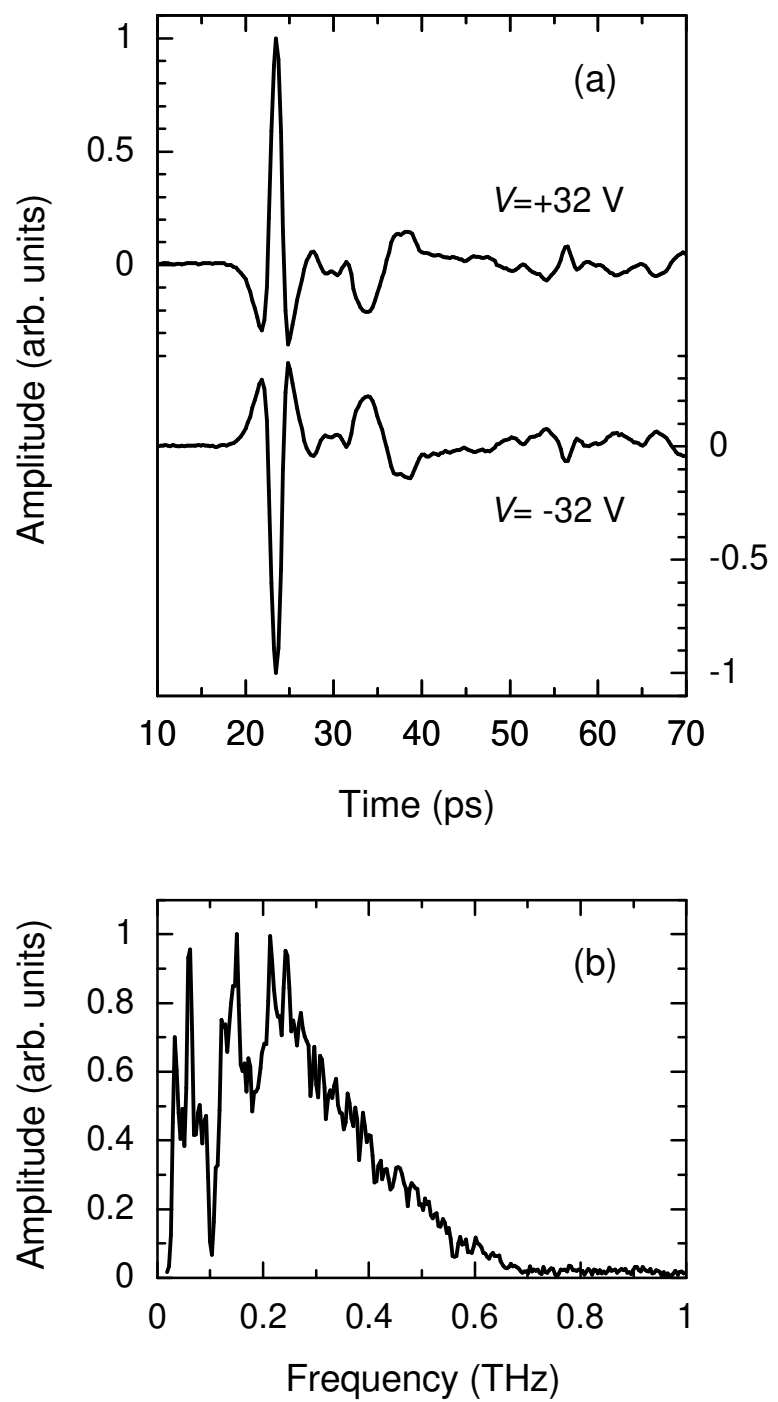


FIG. 1 Kida *et al.*

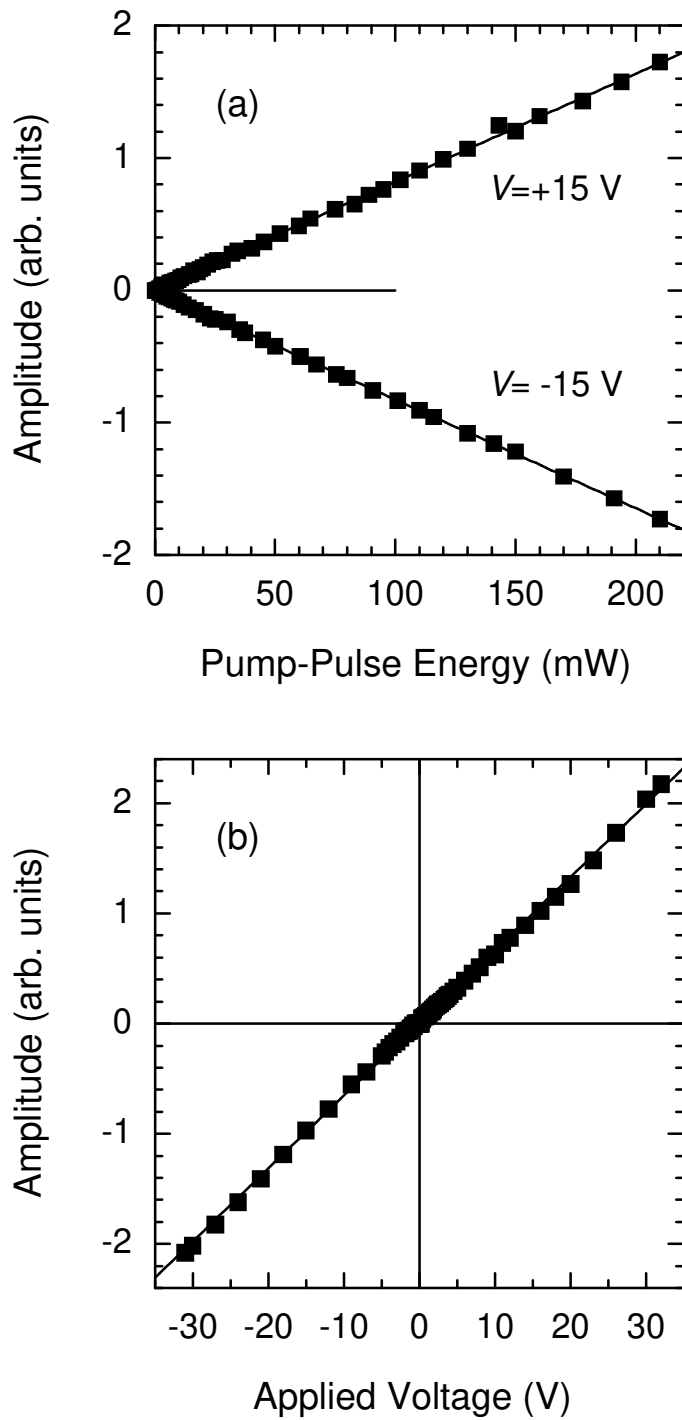


FIG. 2 Kida *et al.*

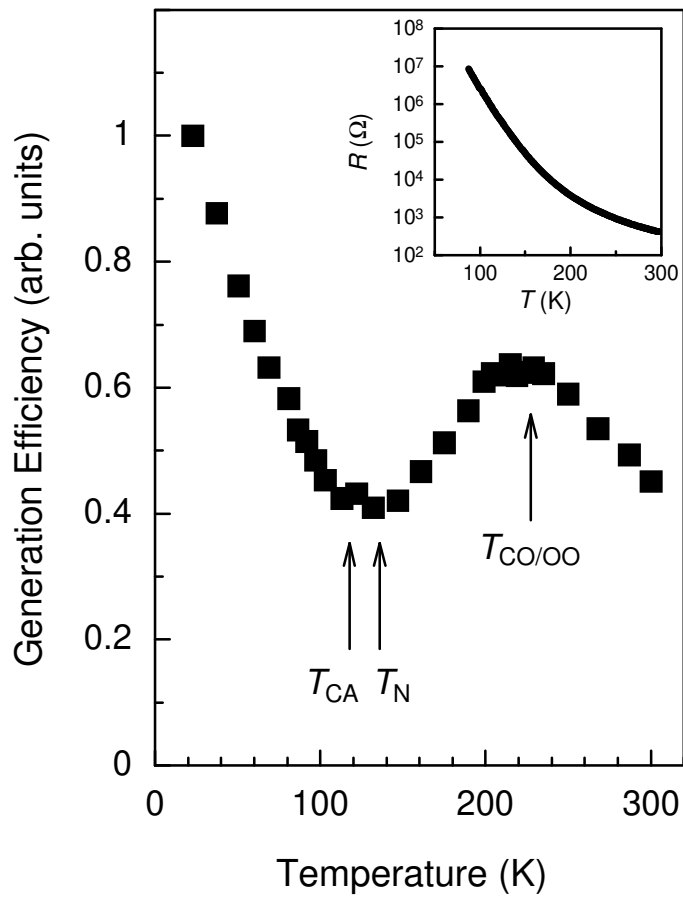


FIG. 3 Kida *et al.*

